Desalination and Water Treatment
www.deswater.com

doi: 10.5004/dwt.2023.29309

285 (2023) 180–188
February

A numerical study of the salt water flow inside a channel with horizontal metal walls subjected to a constant DC voltage realizes a uniform electrostatic field contributing to the desalination of seawater by forcing cations (Na^+) and anions (Cl^-) to deflect: effect of electrostatic field intensity and temperature variation

Jihad Lakouairi[a,*], Zoubair Boulahia[b], Mounir Rifi[a], Abdelhafid Essadki[c], Sara Arsalane[a]

[a]*Laboratory of Network, Computing, Telecommunications and Multimedia, ESTC, Hassan II University of Casablanca, Route d'El Jadida, km 7, BP 8012, Oasis, Casablanca, Morroco, emails: lakouairi.jihad@gmail.com (J. Lakouairi), rifi@email.com (M. Rifi), sara.arsalane@gmail.com (S. Arsalane)*
[b]*Laboratory of Mechanics, Faculty of Sciences Aïn Chock, Hassan II University of Casablanca, BP 5366 Maarif, 20100 Casablanca, Morocco, email: boulahia.zoubair@gmail.com*
[c]*Laboratory of Environment, Process, Energy (LEPE), Hassan II University, ESTC, BP. 8012 Oasis, Casablanca, Morocco, email: essadkiha@gmail.com*

Received 26 July 2022; Accepted 9 January 2023

ABSTRACT

The present article aims to investigate the effect of electrostatic field and temperature on the distribution of chloride and sodium ions during the saltwater flow in a horizontal channel. The change in the intensity of the uniform electric field has been controlled by applying DC high-voltage between the horizontal walls of the channel, where this field creates an electric force that deviate the positive and negative ions towards the walls in opposite directions, which results a large space in the middle of fluid almost free of dissolved salt. The proposed study is formulated with a system of coupled partial differential equations in the Navier–Stokes equation and energy. In addition, the Buongiorno equation was used to study the distribution of ion concentration in seawater. Important results were obtained in this numerical study, including that the increase in the intensity of the electric field and temperature significantly reduced the concentration of cations and anions in a wide area of seawater, thus obtaining a large amount of diluted water. The distribution of sodium and chloride ion concentration, the flow, the horizontal velocity, and the isotherms were modeled under the electrostatic field intensity variation factor and Reynolds number for an accurate, detailed, and clear interpretation.

Keywords: Salt water; Seawater flow; Electric field; Ion concentration; Diluted water

1. Introduction

Most of the ways used to desalinate seawater employ evaporation by changing the phase with the use of a semi-permeable membrane that separates the fresh water from the salty water, therefore companies specializing in desalinating saltwater attempt to produce an inexpensive and quick technology. The effect of various proposed parameters such as flow velocity, temperature variation, and electric field effect has been carefully studied in this article due to the increasing demand for effective and economical water desalination systems. A bibliographical review of past seawater desalination research was undertaken before beginning the suggested investigation in this paper. In the subject

* Corresponding author.

of water desalination, the electric separator techniques for isolating salt from seawater are the most popular. They use magnetic or electrical separation to separate charged particles. An electric or magnetic field can be used to remove dissolved charged particles (ions) from saltwater, which is an electrochemical process that electrolyzes the salt water. The basis of desalination of saline water using an electric or magnetic field is to guide positive and negative particles (ions) towards opposite electrodes. Electrodialysis (ED) technology, which separates ions using electrodes that applies an electrical force that attracts ions to them, is used in many applications, including water desalination. Other technologies, such as reverse osmosis (RO) and multi-stage flash distillation (MFD), are commonly used to desalinate saline water, but they have disadvantages, such as high energy requirements for work and high costs [1]. New methods have been devised to reduce energy consumption by using the electric field effect to desalinate saltwater [2,3]. The researcher Mohammadi et al. [4] have tested the electrodialysis technique to separate the copper ions present in a solution, and they obtained, through the results of the study, the highest percentage of copper ions removal. There are also reviewed works that have tested the efficacy of electrodialysis (ED) are found in these references [5–7]. The electrodialysis reversal (EDR) procedure is used to minimize membrane scaling and fouling by reversing the voltage at regular intervals [8]. There are several studies for desalinating sea water by removing dissolved ions to obtain fresh-water by the effect of the electric field on the movement of ions in electrolyte solutions [9–18]. Alnaimat et al. [19] have studied the effect of electric and magnetic forces on the flow of seawater to separate charged particles, where it was concluded that the flow velocity and electromagnetic force affect the survival time of particles, as well as the separation efficiency. Bartzis et al. [20–23] introduced the electric ion drift (EID) approach, which operates in a similar way to capacitive deionization but does not require membranes or special electrodes. Some important works have been presented in the field of fluid flows and heat transfer. Boulahia et al. [24–32] have investigated natural and mixed convection flow of nanofluid inside a rectangular and wavy cavities containing different block shape by using the generalized Buongiorno's mathematical model.

In this present work, a precise and clear study of the electric field effect applied by two electrodes on the saltwater ions as it flows through horizontal channels will be addressed. The curves, temperature, velocity and distribution of ions will be represented and interpreted.

2. Problem statement

A simplified graph was used to explain the proposed physical problem in this article, which mainly focuses on the flow of seawater through channels subject to temperature variation and electrostatic field. Fig. 1 represents the geometric depiction of the various components of the tested equipment used in this study. A channel of width H and length $L = 5H$ was considered through which the saltwater to be desalinated flows by applying a constant electric voltage (U) and a high potential difference that creates an electric field (E). Fig. 1 shows the cations (Na^+) and anions (Cl^-) represented by red and black particles in seawater and indicate the positioning of the ions to be obtained for desalination. The Boussinesq approximation in the laminar regime was considered which ignored the mass-volume fluctuation except in the amount of the gravitational force, treating seawater as an incompressible Newtonian fluid.

3. Mathematical model

The governing equations including the two-dimensional transient equations of the continuity, momentum, energy, and electric field equations for an incompressible flow are expressed in the following format [33,34]:

$$\frac{\partial u}{\partial x}+\frac{\partial v}{\partial y}=0 \tag{1}$$

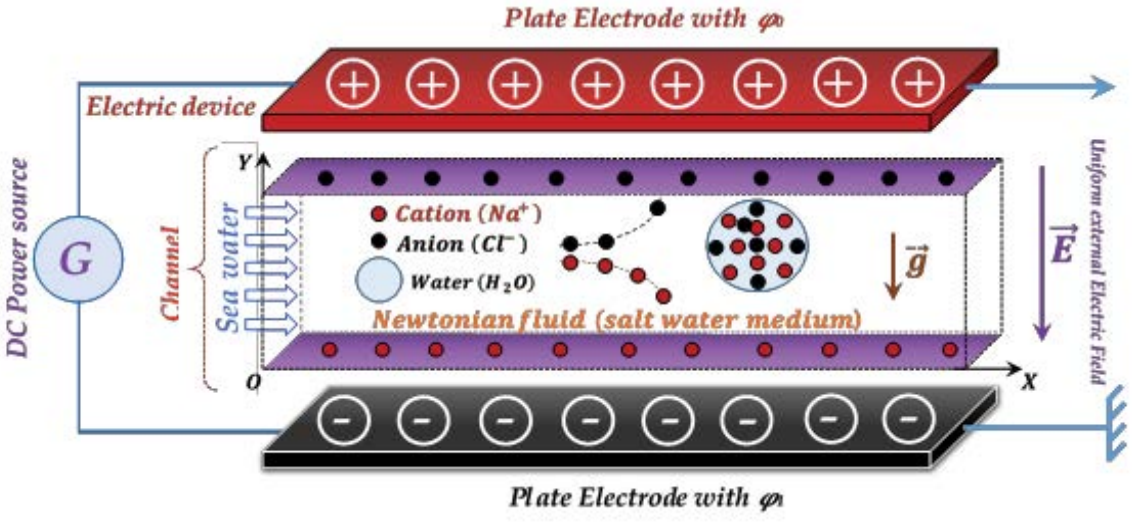

Fig. 1. Geometrical configuration of the studied problem.

$$\frac{\partial u}{\partial t}+u\frac{\partial u}{\partial x}+v\frac{\partial u}{\partial y}=-\frac{1}{\rho_f}\frac{\partial p}{\partial x}+\frac{\mu_f}{\rho_f}\left(\frac{\partial^2 u}{\partial x^2}+\frac{\partial^2 u}{\partial y^2}\right)+\frac{q}{\rho_f}\overline{E_x} \tag{2}$$

$$\frac{\partial v}{\partial t}+u\frac{\partial v}{\partial x}+v\frac{\partial v}{\partial y}=-\frac{1}{\rho_f}\frac{\partial p}{\partial y}+\frac{\mu_f}{\rho_f}\left(\frac{\partial^2 v}{\partial x^2}+\frac{\partial^2 v}{\partial y^2}\right)+\frac{q}{\rho_f}\overline{E_y} \tag{3}$$

$$\frac{\partial T}{\partial t}+u\frac{\partial T}{\partial x}+v\frac{\partial T}{\partial y}=\alpha_f\left(\frac{\partial^2 T}{\partial x^2}+\frac{\partial^2 T}{\partial y^2}\right)+\delta\left[D_B\left(\frac{\partial c}{\partial x}\frac{\partial T}{\partial x}+\frac{\partial c}{\partial y}\frac{\partial T}{\partial y}\right)+D_T\left(\left(\frac{\partial T}{\partial x}\right)^2+\left(\frac{\partial T}{\partial y}\right)^2\right)\right] \tag{4}$$

$$\frac{\partial c}{\partial t}+u\frac{\partial c}{\partial x}+v\frac{\partial c}{\partial y}=D_B\left(\frac{\partial^2 c}{\partial x^2}+\frac{\partial^2 c}{\partial y^2}\right)+D_T\left(\frac{\partial^2 T}{\partial x^2}+\frac{\partial^2 T}{\partial y^2}\right) \tag{5}$$

$$\frac{\partial q}{\partial t}+u\frac{\partial q}{\partial x}+v\frac{\partial q}{\partial y}=D\left(\frac{\partial^2 q}{\partial x^2}+\frac{\partial^2 q}{\partial y^2}\right)-b\left(\overline{E_x}\frac{\partial q}{\partial x}+\overline{E_y}\frac{\partial q}{\partial y}+q\frac{\partial \overline{E_x}}{\partial x}+q\frac{\partial \overline{E_y}}{\partial y}\right) \tag{6}$$

$$\frac{\partial^2 \varphi}{\partial x^2}+\frac{\partial^2 \varphi}{\partial y^2}=-\frac{q}{\varepsilon} \tag{7}$$

With

$$\overline{E_x}=-\frac{\partial \varphi}{\partial x},\overline{E_y}=-\frac{\partial \varphi}{\partial y} \tag{8}$$

$$D_B=\frac{k_B T}{3\pi\mu_f d_p},D_T=\gamma.\frac{\mu_f}{\rho_f T}c,\gamma=0.26\frac{k_f}{2k_f+k_p},\delta=\frac{\rho_p C_{p,p}}{\left(\rho C_p\right)_f} \tag{9}$$

The boundary conditions the problem are written as:

$$u=0,v=0,T=T_c,\frac{\partial c}{\partial y}=-\frac{D_T}{D_B}\frac{\partial T}{\partial y},\quad q=+q_0,\varphi=\varphi_1 \quad \text{at } y=0 \text{ and } 0\le x\le L \tag{10a}$$

$$u=0,v=0,T=T_c,\frac{\partial c}{\partial y}=-\frac{D_T}{D_B}\frac{\partial T}{\partial y},\quad q=-q_0,\varphi=\varphi_0 \quad \text{at } y=H \text{ and } 0\le x\le L \tag{10b}$$

$$u=U_0,v=0,T=T_h,c=C_0,\quad \frac{\partial q}{\partial x}=0,\frac{\partial \varphi}{\partial x}=0 \quad \text{at } x=0 \text{ and } 0\le y\le H \tag{10c}$$

$$u=0,v=0,\frac{\partial T}{\partial x}=0,\frac{\partial c}{\partial x}=0,\quad \frac{\partial q}{\partial x}=0,\frac{\partial \varphi}{\partial x}=0 \quad \text{at } x=L \text{ and } 0\le y\le H \tag{10d}$$

The following dimensionless variables for natural convection are defined based on properties of pure fluid:

$$\tau=\frac{t}{H/U_{\text{ref}}},X=\frac{x}{H},Y=\frac{y}{H},U=\frac{u}{U_{\text{ref}}},V=\frac{v}{U_{\text{ref}}},$$
$$P=\frac{p}{\rho_f U_{\text{ref}}^2},\theta=\frac{T-T_c}{T_h-T_c},C=\frac{c}{C_0},Q=\frac{q}{q_0},E=\frac{\overline{E}}{\Delta\varphi/H},$$
$$\phi=\frac{\varphi-\varphi_1}{\varphi_0-\varphi_1}, \tag{11}$$

Where U_{ref} is considered to be U_0 for forced convection.

Dimensionless numbers for the system are defined as:

$$\text{Re}=\frac{U_0 H}{\nu_f},\text{Pr}=\frac{\nu_f}{\alpha_f},\text{Le}=\frac{k_f}{\left(\rho C_p\right)_p D_B c_0},\text{Sc}=\frac{\mu_f}{\rho_f D_B},$$
$$N_{\text{BT}}=\frac{D_B c_0}{D_T\Delta T},\text{Pr}_E=\frac{\nu_f}{b\Delta\varphi},N_E=\frac{q_0 H^2}{\varepsilon\Delta\varphi},S_E=\frac{q_0\Delta\varphi}{\rho_f U_0^2},D_e=\frac{\nu_f}{D} \tag{12}$$

The governing Eqs. (1)–(7) are written in the following dimensionless form:

$$\frac{\partial U}{\partial X}+\frac{\partial V}{\partial Y}=0 \tag{13}$$

$$\frac{\partial U}{\partial \tau}+U\frac{\partial U}{\partial X}+V\frac{\partial U}{\partial Y}=-\frac{\partial P}{\partial X}+\frac{1}{\text{Re}}\left(\frac{\partial^2 U}{\partial X^2}+\frac{\partial^2 U}{\partial Y^2}\right)+S_E\text{QE}_x \tag{14}$$

$$\frac{\partial V}{\partial \tau}+U\frac{\partial V}{\partial X}+V\frac{\partial V}{\partial Y}=-\frac{\partial P}{\partial Y}+\frac{1}{\text{Re}}\left(\frac{\partial^2 V}{\partial X^2}+\frac{\partial^2 V}{\partial Y^2}\right)+S_E QE_y \tag{15}$$

$$\frac{\partial \theta}{\partial \tau}+U\frac{\partial \theta}{\partial X}+V\frac{\partial \theta}{\partial Y}=\frac{1}{\text{Pr}\cdot\text{Re}}\left\{\begin{array}{l}\left(\frac{\partial^2\theta}{\partial X^2}+\frac{\partial^2\theta}{\partial Y^2}\right)\\ +\frac{1}{\text{Le}}\left[\begin{array}{l}\frac{\partial C}{\partial X}\cdot\frac{\partial\theta}{\partial X}+\frac{\partial C}{\partial Y}\cdot\frac{\partial\theta}{\partial Y}\\ +\frac{1}{N_{\text{BT}}}\left(\frac{\partial\theta}{\partial X}\right)^2+\left(\frac{\partial\theta}{\partial X}\right)^2\end{array}\right]\end{array}\right\} \tag{16}$$

$$\frac{\partial C}{\partial \tau}+U\frac{\partial C}{\partial X}+V\frac{\partial C}{\partial Y}=\frac{1}{\text{Re}\cdot\text{Sc}}\left[\begin{array}{l}\left(\frac{\partial^2 C}{\partial X^2}+\frac{\partial^2 C}{\partial Y^2}\right)\\ +\frac{1}{N_{\text{BT}}}\left(\frac{\partial^2\theta}{\partial X^2}+\frac{\partial^2\theta}{\partial Y^2}\right)\end{array}\right] \tag{17}$$

$$\frac{\partial Q}{\partial \tau}+U\frac{\partial Q}{\partial X}+V\frac{\partial Q}{\partial Y}=\frac{1}{\text{Re}\cdot\text{De}}\left(\frac{\partial^2 Q}{\partial X^2}+\frac{\partial^2 Q}{\partial Y^2}\right)-\frac{1}{\text{Re}\cdot\text{Pr}_E}\left(E_x\frac{\partial Q}{\partial X}+E_y\frac{\partial Q}{\partial Y}+Q\frac{\partial E_x}{\partial X}+Q\frac{\partial E_y}{\partial Y}\right) \tag{18}$$

$$\frac{\partial^2\phi}{\partial X}+\frac{\partial^2\phi}{\partial Y^2}=-N_E\cdot Q \tag{19}$$

With

$$E_x = -\frac{\partial \phi}{\partial X}, E_y = -\frac{\partial \phi}{\partial Y} \tag{20}$$

Dimensionless form of the boundary conditions can be written as:

$$U = 0, V = 0, \theta = 0, \frac{\partial C}{\partial Y} = -\frac{1}{N_{BT}}\frac{\partial \theta}{\partial Y},$$
$$Q = +1, \phi = 0 \qquad \text{at } Y = 0 \text{ and } 0 \le X \le 5 \tag{21a}$$

$$U = 0, V = 0, \theta = 0, \frac{\partial C}{\partial Y} = -\frac{1}{N_{BT}}\frac{\partial \theta}{\partial Y},$$
$$Q = -1, \phi = 1 \qquad \text{at } Y = 1 \text{ and } 0 \le X \le 5 \tag{21b}$$

$$U = 1, V = 0, \theta = 1, C = 1,$$
$$\frac{\partial Q}{\partial X} = 0, \frac{\partial \phi}{\partial X} = 0 \qquad \text{at } X = 0 \text{ and } 0 \le Y \le 1 \tag{21c}$$

$$U = 0, V = 0, \frac{\partial \theta}{\partial X} = 0, \frac{\partial C}{\partial X} = 0,$$
$$\frac{\partial Q}{\partial X} = 0, \frac{\partial \phi}{\partial X} = 0 \qquad \text{at } X = 1 \text{ and } 0 \le Y \le 1 \tag{21d}$$

4. Numerical details

The dimensionless governing equations [Eqs. (13)–(19)] and boundary conditions [Eq. (21)] are based on a finite volume formulation on a staggered grid, as presented by Patankar [35]. The linked pressure–velocity equation is solved using SIMPLE (Semi-Implicit Method for Pressure Linked Equations), whereas the convective components are solved using Spalding's Hybrid Differencing Scheme (HDS) [36].

The integration of the dimensionless governing Eqs. (13)–(19) over a two-dimensional control volume CV is a crucial step in the finite volume technique. For the variable, the integration of the transport equation may be expressed in a general form as follows:

$$\int_{CV} \frac{\partial \phi}{\partial t} dV + \int_{CV} \left(U \frac{\partial \phi}{\partial X} + V \frac{\partial \phi}{\partial Y} \right) dV = \int_{CV} \Gamma \left(\frac{\partial^2 \phi}{\partial X^2} + \frac{\partial^2 \phi}{\partial Y^2} \right) dV + \int_{CV} S \, dV \tag{22}$$

$dV = dX \cdot dY$, ($dZ = 1$), where S is the source term.

The algebraic finite volume equations for the momentum and energy equations are stated as follows after integration:

$$a_P \phi_P = a_W \phi_W + a_E \phi_E + a_S \phi_S + a_N \phi_N + S_\phi \tag{23}$$

where P, W, E, N, S successively signify cell location, west face of the control volume, east face of the control volume, north face of the control volume, and south face of the control volume CV (Fig. 2).

On equation systems, the TDMA (Tri-Diagonal Matrix Algorithm) approach [35] is used line by line until the total of the residuals is less than 10^{-6}. The FORTRAN program was used to implement the proposed algorithm.

4.1. Grid independence study

A planned research of grid independence is carried out in order to ensure reliable numerical results. The effect of high voltage (10 kV) on a channel filled with saltwater is measured in Reynolds number (Re = 600). The desalination quality test is well checked for the length $L = 5H$, where it will be discussed further in the upcoming works. Table 1 shows the maximum horizontal velocity achieved using various non-uniform grid numbers. As can be seen in the table, a non-uniform 51 × 301 grid is adequate for the numerical calculation.

4.2. Validations

The numerical approach is confirmed by comparing it to the distribution contours of nanoparticles of Garoosi et al. [34], Sheikhzade et al. [37] and numerical results of Khanafer et al. [38] (Gr = 104, $C = 0.1$ and Pr = 6.8 (Cu–Water)) as shown in Fig. 3. The results of this study are extremely similar to those found in the literature.

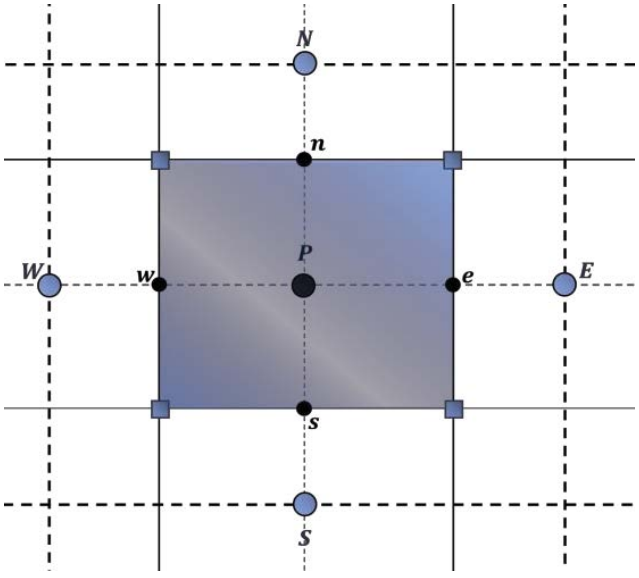

Fig. 2. The volume centers are designated with uppercase letters, whereas the faces are labeled with lowercase letters in a typical control volume CV.

Table 1
Maximum horizontal velocity for different grids Re = 600

Grid size	31 × 101	41 × 201	51 × 301	61 × 401
U_{max}	1.182	1.213	1.251	1.252

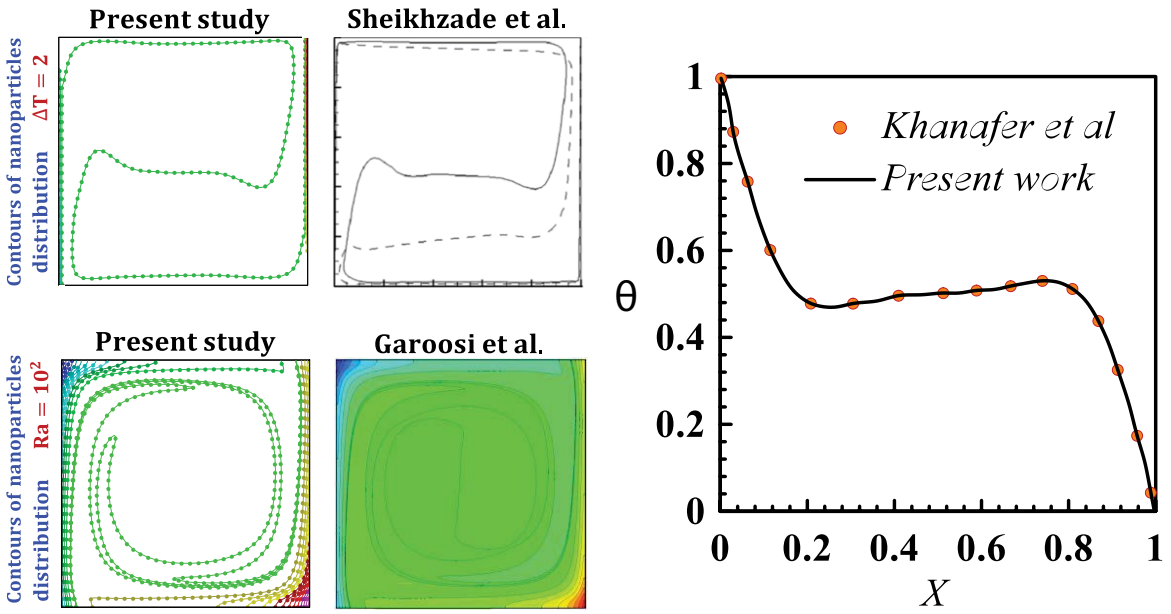

Fig. 3. Comparison of the present study with the distribution contours of nanoparticles of Garoosi et al. [34], Sheikhzade et al. [37] and numerical results of Khanafer et al. [38] (Gr = 104, C = 0.1 and Pr = 6.8 (Cu–Water)).

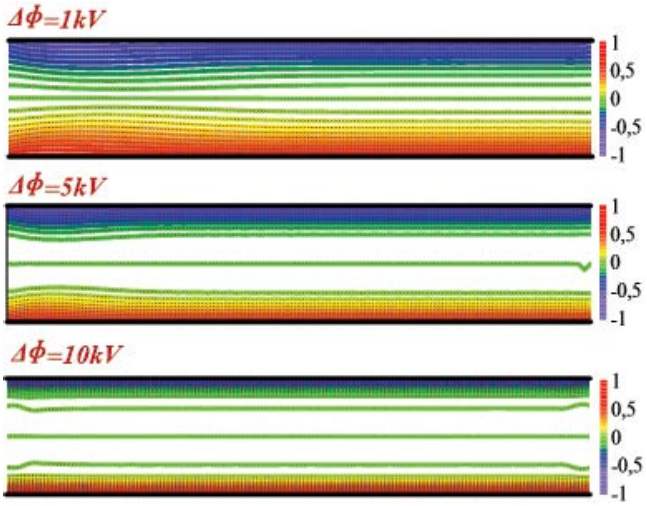

Fig. 4. The influence of supplied voltage (1 kV ≤ Δϕ ≤ 10 kV) on electric density distribution.

5. Results and discussion

This section examined the numerical analysis of the seawater flow inside a channel under the effect of an electric field generated by two high-voltage plates. This numerical modeling highlighted the influence of supplied voltage (1 kV ≤ Δϕ ≤ 10 kV) on electrical density distribution, as well as the impact of Reynolds number (100 ≤ Re ≤ 600) number on horizontal velocity, streamlines, isotherms, and concentration.

Through the obtained results in Fig. 4, we can clearly remark the effect of the high voltage difference on the distribution of positive and negative electric densities, which represent cations (positive ions Na^+) and anions (negative ions Cl^-), respectively. The distribution of the electric density was represented for different values of the high potential difference between 1 and 10 kV under a fixed value of the Reynolds number Re = 50. Fig. 4 shows that the position of the negative electric density (Cl^-) is on the upper positive electrode, and the positive electric density (Na^+) is on the lower negative electrode. By analyzing the distribution of electric density, we can notice that studied fluid (seawater) has an electrically neutral zone, where the electric density is zero. In this illustration, the fluid with an electrical density that is lower than or equal to zero is represented by the green color and is thought to be diluted water. When the potential difference is equal to 1 kV, we note that the distribution of electric density in seawater is uniform, as the percentage of this region does not exceed the zero electric density (diluted water) 20%. By gradually raising the value of the potential difference from 1 to 10 kV, we notice the overlapping and crowding of the positive and negative electrical density in the lower and upper wall, which makes the size of the area containing diluted water increase, reaching approximately 50% for the potential difference 5 kV and 70% for the 10 kV.

Fig. 5 depicts a representation of electric density variation in the center of the channel that was previously illustrated in Fig. 4. The obtained results show that when the potential difference increases from 1 to 10 kV, the electric density changes significantly and its representative curve becomes straight in the center. This demonstrates the presence of a zero electrical density fluid (electrically neutral region), which represents diluted water, and implies that there is an equal number of opposing charges present at very low concentrations due to the potential difference applied between the electrodes (The ion concentration distribution results will be discussed in the next paragraph and will verify the almost total migration of ions from the medium to the

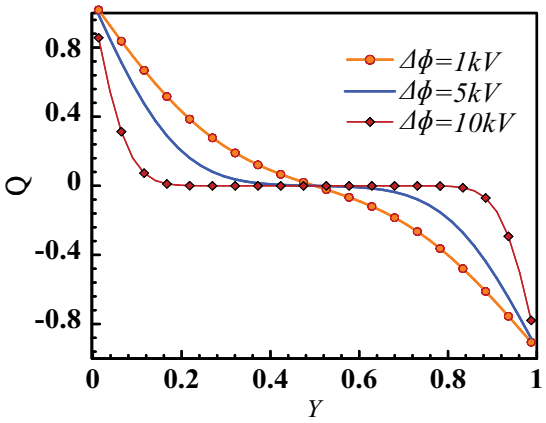

Fig. 5. The electric density variation (Q) in the middle of the channel at (X = 0.5, Re = 50 and 1 kV ≤ Δϕ ≤ 10 kV).

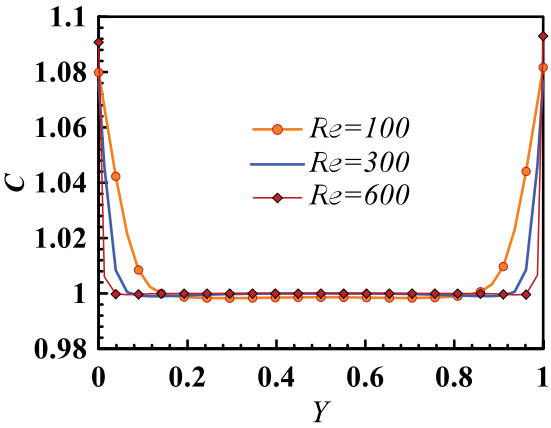

Fig. 7. The concentration variation (C) in the middle of the channel at (Re = 100, 300, and 600, Δϕ = 10 kV).

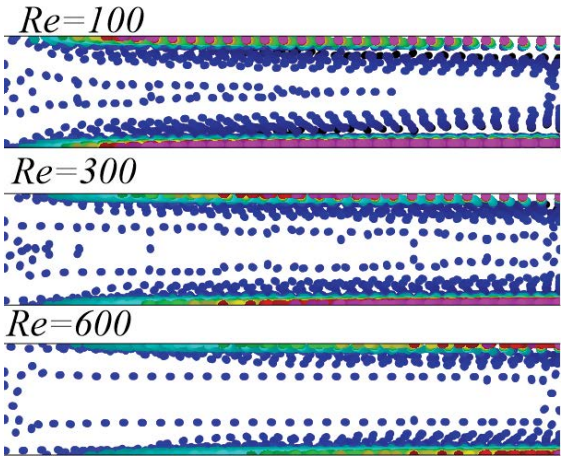

Fig. 6. The iso-concentration distribution for different Reynolds number (Re = 100, 300, and 600) at Δϕ = 10 kV.

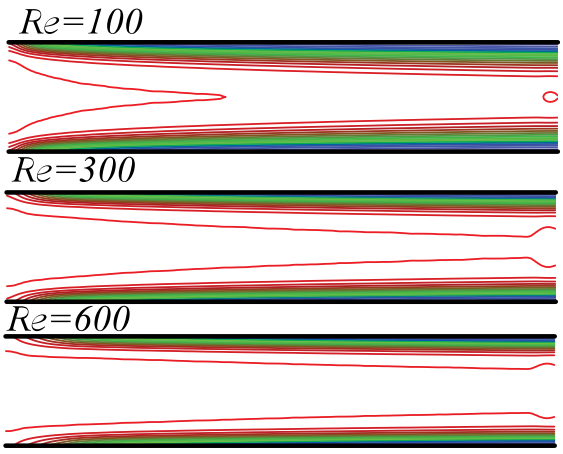

Fig. 8. The isotherms distribution for different Reynolds number (Re = 100, 300, and 600) at Δϕ = 10 kV.

regions near the electrodes). This confirms that the potential difference has a great effect on salt separation from seawater.

Fig. 6 represents the distribution of particle concentration in seawater as it flows through horizontal channels for different Reynolds numbers (100 ≤ Re ≤ 600). It can be seen that the particles (ions) are located near the upper and lower horizontal walls of the channels due to the change in the velocity and temperature of the fluid. It's also worth to note that there are two zones: one with low particle concentration concentrated in the medium, and the other with high particle concentration close to the horizontal walls, considering that the size of this region grows as the Reynolds number rises from 100 to 600.

Fig. 7 improves the results reported in Fig. 6 for the region with constant particle concentration. This figure also shows that the particle concentration varies near the wall, indicating that the particles are near these walls (Y = 0 and Y = 1)), and that there is straight and constant component of the particle concentration curve, whose width grows as the Reynolds number increases.

Fig. 8 represents the isotherms distribution in seawater within a channel in terms of the different Reynolds number.

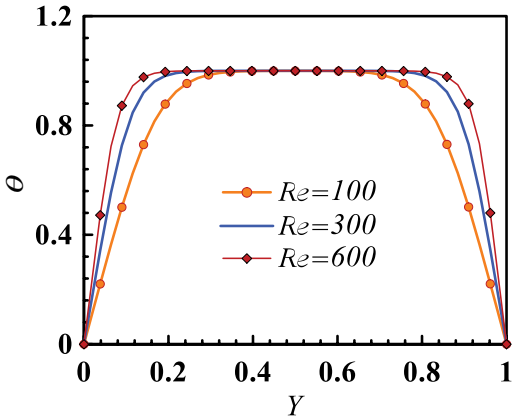

Fig. 9. The temperature variation (θ) in the middle of the channel at (Re = 100, 300, and 600, Δϕ = 10 kV).

We notice that the concentration of the isotherms overlap in the upper and lower walls, where they jostle with each other with the increase in the Reynolds number, which leads to the emergence of a region of fluid with the same temperature.

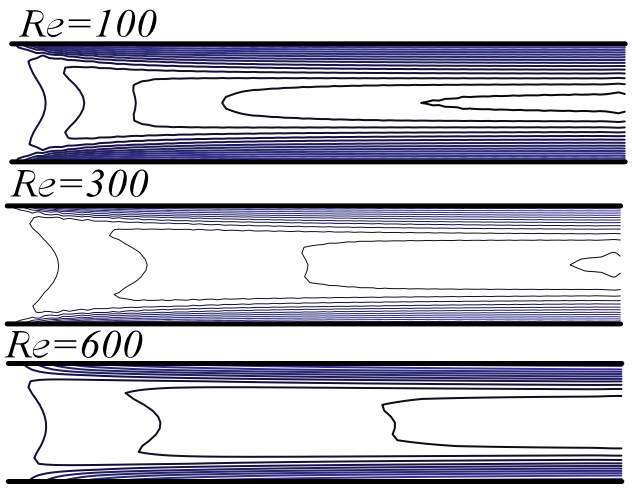

Fig. 10. The horizontal velocity distribution for different Reynolds number (Re = 100, 300, and 600) at Δϕ = 10 kV.

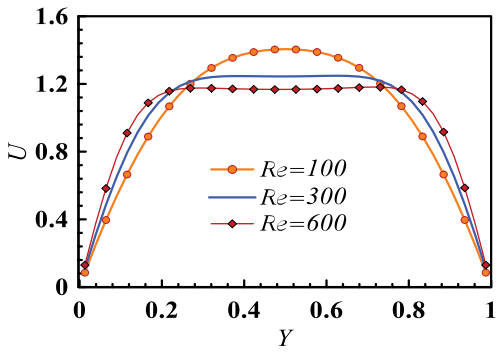

Fig. 11. The horizontal velocity variation (*U*) in the middle of the channel at (Re = 100, 300, and 600, Δϕ = 10 kV).

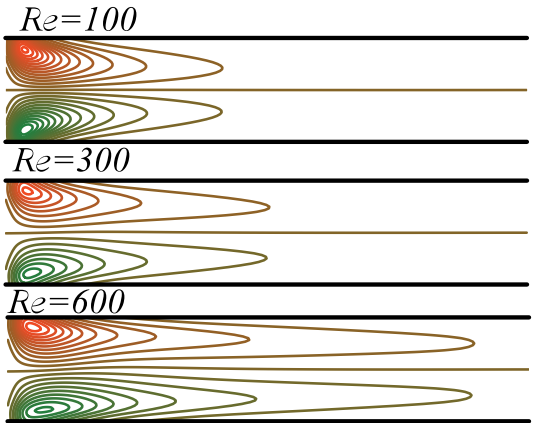

Fig. 12. The vertical velocity (*V*) distribution for different Reynolds number (Re = 100, 300, and 600) at Δϕ = 10 kV.

Fig. 9 shows that the temperature change is located close to the upper and lower walls, and there is a region of temperature curve that is straight and constant whose width grows as well with the increase in the Reynolds number.

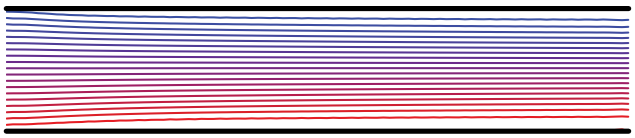

Fig. 13. The streamlines distribution for (Re = 600) at Δϕ = 10 kV.

Fig. 10 shows the horizontal velocity distribution for different Reynolds number (Re = 100, 300, and 600) at Δϕ = 10 kV. We can clearly see that the iso-velocity affected significantly by the rising of Reynolds number. The maximum values of horizontal velocity are situated on the center of fluid. It is noticed that the zone with constant velocity increases by rising the Reynolds number which can be plainly seen in the Fig. 11, for Re = 600, where the curve of the horizontal velocity is straight and constant.

Figs. 12 and 13 show the distribution of vertical velocity and streamline. It can be seen in Fig. 12 that the vertical velocity distribution is characterized by two cells which its form change significantly by Reynolds number.

6. Conclusions

This article looked at a numerical simulation of seawater flow inside a channel under the influence of an electric field generated by two high-voltage plates. The numerical modeling showed the effect of applied voltage on electrical density distribution, as well as the effect of Reynolds number on horizontal velocity, streamlines, isotherms, and concentration. The major findings are as follows:

- the position of the negative electric density (Cl^-) is on the upper positive electrode, as for the positive electric charge (Na^+) it is located on the lower negative electrode.
- By gradually raising the value of the potential difference from 1 to 10 kV, we notice the overlapping and crowding of the positive and negative electrical density in the lower and upper wall, which makes the area containing diluted water increase, reaching approximately 50% for the potential difference 5% and 70% for the 10 kV.
- The particles are located near the upper and lower horizontal walls of the channels and there's a zone in the fluid medium with a low particle concentration.
- Isotherms jostle with each other to form a region of fluid with the same temperature. Temperature changes are placed close to the upper and lower walls, and there is a straight and constant section of particle concentration curve whose width grows as the Reynolds number increases.
- The iso-velocity affected significantly by the rising of Reynolds number. The maximum values of horizontal velocity are situated on the center of fluid which is straight and constant.

Symbols

b	—	Ionic mobility, $m^2/s{\cdot}V$
C_p	—	Specific heat, J/kg·K
d	—	Diameter, m
D	—	Charge diffusion coefficient, m^2/s

D_B	—	Brownian coefficient, kg/m·s
D_e	—	Diffusion number
D_T	—	Thermophoresis coefficient, kg/m·s·K
c	—	Concentration of particles
C	—	Dimensionless concentration
$\tilde{E}$	—	Electric field, V/m
E	—	Dimensionless electric field
H	—	Height, m
k	—	Thermal conductivity, W/m·K
k_B	—	Boltzmann constant, J/K
L	—	Length, m
Le	—	Lewis number
N_E	—	Electric field number
N_{BT}	—	Ratio of Brownian and thermophoretic diffusivities
p	—	Pressure, N/m^2
P	—	Dimensionless pressure
Pr	—	Prandtl number
Pr_E	—	Electric Prandtl number
q	—	Electric charge density, C/m^3
Q	—	Dimensionless electric charge density
Re	—	Reynolds number
$S(\phi)$	—	Source term related to transport variable ϕ
Sc	—	Schmidt number
S_E	—	Lorentz force number
t	—	Time, s
T	—	Temperature, K
u, v	—	Dimensional x and y-components of velocity, m/s
U, V	—	Dimensionless velocity components
x, y	—	Cartesian coordinates, m
X, Y	—	Dimensionless cartesian coordinates

Greek symbols

α	—	Thermal diffusion coefficient, m^2/s
θ	—	Dimensionless temperature
ν	—	Kinematic viscosity, m^2/s
μ	—	Dynamic viscosity, kg/m·s
ρ	—	Density, kg/m^3
φ	—	Electric field potential, V
ϕ	—	General transport field variables
δ	—	Ratio of particle and fluid heat capacitance, J/K·m^3
γ	—	Thermophoretic coefficient
ε	—	Dielectric permittivity, F/m
τ	—	Dimensionless time
Γ	—	Diffusion coefficient of φ

Subscripts

0	—	Reference
c	—	Cold
f	—	Fluid
h	—	Hot
f	—	Fluid
p	—	Particle

References

[1] D. Zarzo, D. Prats, Desalination and energy consumption. What can we expect in the near future?, Desalination, 427 (2018) 1–9.

[2] L. Gu, X.G. Chen, X.D. Liu, W. Liu, Ion distribution in saltwater under high-voltage static electric field, Adv. Mater. Res., 361–363 (2012) 865–869.

[3] L. Gu, Simulation of ion distribution on both sides of insulation film in saltwater under static electric field, Adv. Mater. Res., 538–541 (2012) 110–115.

[4] T. Mohammadi, A. Moheb, M. Sadrzadeh, A. Razmi, Separation of copper ions by electrodialysis using Taguchi experimental design, Desalination, 169 (2004) 21–31.

[5] T. Mohammadi, A. Kaviani, Water shortage and seawater desalination by electrodialysis, Desalination, 158 (2003) 267–270.

[6] P. Murray, Electrodialysis and Electrodialysis Reversal, AWWA Man. M38, Colorado, 1999.

[7] W.S.W. Ho, K.K. Sirkar, Membrane Handbook, Springer Science Business+Media, New York, 1992.

[8] P. Murray, Electrodialysis and Electrodialysis Reversal-Manual of Water Supply Practices, American Water Works Association, Colorado, 1995.

[9] M.E. Suss, S. Porada, X. Sun, P.M. Biesheuvel, J. Yoon, V. Presser, Water desalination via capacitive deionization: what is it and what can we expect from it?, Energy Environ. Sci., 8 (2015) 2296–2319.

[10] M. Sheikholeslami, M.A. Sheremet, A. Shafee, Z. Li, CVFEM approach for EHD flow of nanofluid through porous medium within a wavy chamber under the impacts of radiation and moving walls, J. Therm. Anal. Calorim., 138 (2019) 573–581.

[11] I.G. Tironi, R. Sperb, P.E. Smith, W.F. Van Gunsteren, A generalized reaction field method for molecular dynamics simulations, J. Chem. Phys., 102 (1995) 5451–5459.

[12] F. Sofos, T.E. Karakasidis, D. Spetsiotis, Molecular dynamics simulations of ion separation in nano-channel water flows using an electric field, Mol. Simul., 45 (2019) 1395–1402.

[13] S. Murad, The role of external electric fields in enhancing ion mobility, drift velocity, and drift-diffusion rates in aqueous electrolyte solutions, J. Chem. Phys., 134 (2011) 1–7.

[14] A. Morro, R. Drouot, G.A. Maugin, Thermodynamics of polyelectrolyte solutions in an electric field, J. Non-Equilib. Thermodyn., 10 (1985) 131–144.

[15] K.A. Maerzke, J. Ilja Siepmann, Effects of an applied electric field on the vapor-liquid equilibria of water, methanol, and dimethyl ether, J. Phys. Chem. B, 114 (2010) 4261–4270.

[16] M.J. Gordon, X. Huang, S.L. Pentoney, R.N. Zare, Capillary electrophoresis, Science, 242 (1988) 224–228.

[17] H.J. Bakker, Structural dynamics of aqueous salt solutions, Chem. Rev., 108 (2008) 1456−1473.

[18] M.R. Wright, An Introduction to Aqueous Electrolyte Solutions, John Wiley & Sons, England, 2007.

[19] F. Alnaimat, E. Alhseinat, F. Banat, V. Mittal, Electromagnetic-mechanical desalination: mathematical modeling, Desalination, 380 (2016) 75–84.

[20] V. Bartzis, I.E. Sarris, A theoretical model for salt ion drift due to electric field suitable to seawater desalination, Desalination, 473 (2020) 114163, doi: 10.1016/j.desal.2019.114163.

[21] V. Bartzis, I.E. Sarris, Electric field distribution and diffuse layer thickness study due to salt ion movement in water desalination, Desalination, 490 (2020) 114549, doi: 10.1016/j.desal.2020.114549.

[22] V. Bartzis, I.E. Sarris, Time evolution study of the electric field distribution and charge density due to ion movement in salty water, Water, 13 (2021) 2185, doi: 10.3390/w13162185.

[23] V. Bartzis, G. Ninos, I.E. Sarris, Water purification from heavy metals due to electric field ion drift, Water, 14 (2022) 2372, doi: 10.3390/w14152372.

[24] Z. Boulahia, A. Wakif, R. Sehaqui, Modeling of free convection heat transfer utilizing nanofluid inside a wavy enclosure with a pair of hot and cold cylinders, Front. Heat Mass Transfer, 8 (2017) 1–10.

[25] Z. Boulahia, A. Wakif, A.J. Chamkha, R. Sehaqui, Numerical study of natural and mixed convection in a square cavity filled by a Cu-water nanofluid with circular heating and cooling cylinders, Mech. Ind., 18 (2017) 502, doi: 10.1051/meca/2017021.

[26] Z. Boulahia, A. Wakif, R. Sehaqui, Numerical study of mixed convection of the nanofluids in two-sided lid-driven square

cavity with a pair of triangular heating cylinders, J. Eng., 2016 (2016) 1–8.
[27] Z. Boulahia, A. Wakif, A.J. Chamkha, C.H. Amanulla, R. Sehaqui, Effects of wavy wall amplitudes on mixed convection heat transfer in a ventilated wavy cavity filled by copper-water nanofluid containing a central circular cold body, J. Nanofluids, 8 (2019) 1170–1178.
[28] Z. Boulahia, A. Wakif, A.J. Chamkha, R. Sehaqui, Numerical study of forced, mixed and natural convection of nanofluids inside a ventilated cavity containing different shapes of cold block, J. Nanofluids, 8 (2019) 1–9.
[29] Z. Boulahia, A. Wakif, R. Sehaqui, Numerical modeling of natural convection heat transfer in a wavy wall enclosure filled by a Cu-water nanofluid with a square cooler, J. Nanofluids, 6 (2017) 324–333.
[30] Z. Boulahia, A. Wakif, R. Sehaqui, Finite volume analysis of free convection heat transfer in a square enclosure filled by a cu-water nanofluid containing different shapes of heating cylinder, J. Nanofluids, 6 (2017) 761–768.
[31] Z. Boulahia, C. Boulahia, R. Sehaqui, Two-phase computation of free convection and entropy generation inside an enclosure filled by a hybrid Al_2O_3-TiO_2-Cu water nanofluid having a corrugated heat source using the generalized Buongiorno's mathematical model: employ, Mater. Today Proc., 30 (2020) 1056–1067.
[32] Z. Boulahia, A. Wakif, R. Sehaqui, Heat transfer and cu-water nanofluid flow in a ventilated cavity having central cooling cylinder and heated from the below considering three different outlet port locations, Front. Heat Mass Transfer, 11 (2018) 1–10.
[33] M. Sheikholeslami, T. Hayat, A. Alsaedi, S. Abelman, Numerical analysis of EHD nanofluid force convective heat transfer considering electric field dependent viscosity, Int. J. Heat Mass Transfer, 108 (2017) 2558–2565.
[34] F. Garoosi, S. Garoosi, K. Hooman, Numerical simulation of natural convection and mixed convection of the nanofluid in a square cavity using Buongiorno model, Powder Technol., 268 (2014) 279–292.
[35] S.V. Patankar, Numerical Heat Transfer and Fluid Flow, Taylor and Francis, London, 1980.
[36] D.B. Spalding, A novel finite difference formulation for differential expressions involving both first and second derivatives, Int. J. Numer. Methods Eng., 4 (1972) 551–559.
[37] G.A. Sheikhzadeh, M. Dastmalchi, H. Khorasanizadeh, Effects of nanoparticles transport mechanisms on Al_2O_3-water nanofluid natural convection in a square enclosure, Int. J. Therm. Sci., 68 (2013) 79–93.
[38] K. Khanafer, K. Vafai, M. Lightstone, Buoyancy-driven heat transfer enhancement in a two-dimensional enclosure utilizing nanofluids, Int. J. Heat Mass Transfer, 46 (2003) 3639–3653.